International Journal of Non–Linear Mechanics 187 (2026) 105362

Contents lists available at ScienceDirect

International Journal of Non-Linear Mechanics

journal homepage: www.elsevier.com/locate/nlm

On the effect of planar dynamics and resonance on vibration-induced friction modulation

E. Sulollari *, K.N. van Dalen, A. Cabboi

Department of Engineering Structures, Faculty of Civil Engineering and GeoSciences, Delft University of Technology, Stevinweg 1, 2628CN Delft, The Netherlands

ARTICLE INFO

Keywords:
Transverse stiffness
Effective friction
Dynamic friction
Nonlinear damping

ABSTRACT

Numerous theoretical and experimental studies have explored the effect of external excitation in modulating friction forces. To align with experimental findings, various friction models have been employed, with dynamic constitutive laws of friction often showing better correlations, though parameter tuning is always required for each different case. In this work, the focus is on enhancing the overall system dynamics rather than increasing the complexity of the friction law, with the aim of providing a better understanding of how system dynamics influence friction modulation under vibration. Specifically, two cases are investigated. A first one-degree-of-freedom case explores a resonant (and nearby resonance) case with a weak and strong friction force, for which an enhanced implicit expression for the velocity response (needed to compute the modulated friction quantity) is provided. The second case investigates the influence of transverse stiffness on friction modulation in a two-degree-of-freedom system subjected to combined longitudinal and transverse loading. On a qualitative basis, this study indicates that the results obtained using dynamic friction laws can also be obtained by employing Amonton-Coulomb's law, provided the system's dynamics is captured at a more detailed level.

1. Introduction

Friction forces not only resist motion but also interact dynamically with external disturbances or fluctuating loads. From the system dynamics perspective, this interaction can amplify, dissipate, or modulate the system's vibrations, strongly influencing stability and performance. However, it can also significantly alter the friction force behaviour itself, especially if the goal is to either characterize the friction force through measurements, or control it. Examples of techniques meant to control the friction behaviour by means of an applied oscillatory force include wire drawing [1], cutting [2], press forming [3], and other machining processes, slip-joint decommissioning [4,5], pile driving [6] and surface haptics technologies [7].

Since the 1950s, several studies on the effect of vibrations on friction have been performed, including experimental and theoretical ones. Some of them investigated the reduction of the friction force due to ultrasonic vibrations applied parallel and/or perpendicularly to the sliding direction and developed simple models used to match the experimental results to theoretical predictions [8–10]. These models consisted of two bodies sliding over each other, with the friction force assumed to follow Amonton-Coulomb's law. Other studies considered more complex friction laws. Thomsen, for example, considered the Stribeck law and studied the effect of harmonic excitation on changing friction forces and quenching self-excited vibrations [11]. Michaux and coworkers also considered the Stribeck law and investigated the effect of the waveform of different periodic signals on the effectiveness of longitudinal high-frequency excitation to cancel friction-induced oscillations [12]. In general, in the above-mentioned studies, the reduction or modulation of the friction force is quantified by means of averaging the friction force throughout one cycle of vibration. A reduction of the averaged friction terms can be observed whenever a change in the direction of the net friction force vector occurs, with respect to the direction of the uniform motion of one of the contacting surfaces.

A series of numerical and experimental investigations have been performed by Leus and Gutowski, focusing on the use of a longitudinal oscillatory load to reduce the averaged friction force. In the early 2000s, they showed that using the Dahl model, a dynamic constitutive law of friction in which the interface shear stiffness contribution provided by the asperities is modelled by means of micro-springs, the friction force could be reduced independently of whether a change in the direction of the net friction force vector is observed [13]. Later on, considering again longitudinal harmonic loads, they compared numerical results of the averaged friction term, obtained assuming the Dahl's and Dupont's models and the classical Amonton-Coulomb's friction law, with experimental data. The best correlations were observed using the Dahl's friction model [14]. Numerical and experimental studies

* Corresponding author.
E-mail addresses: E.Sulollari@tudelft.nl (E. Sulollari), K.N.vanDalen@tudelft.nl (K.N. van Dalen), A.Cabboi@tudelft.nl (A. Cabboi).

https://doi.org/10.1016/j.ijnonlinmec.2026.105362
Received 5 December 2025; Received in revised form 11 March 2026; Accepted 21 March 2026
Available online 23 March 2026

were performed to investigate the effect of transverse vibrations as well [15]. More recently, a computational model was developed to study the friction force reduction under longitudinal loading applied at an arbitrary direction, assuming again dynamic friction models and comparing the numerical results to experimental ones [16].

As mentioned above, in the existing studies, dynamic friction models, such as the Dahl or Dupont models, are incorporated for theoretical predictions to better correlate with experimental results. These dynamic friction models account for the contact surface deformation by linking the friction force during the pre-sliding phase to an empirical longitudinal contact stiffness parameter. Even though such models are suitable for matching experimental results, their model parameters cannot always be physically linked to measurable surface properties and need to be constantly updated to match new measurements. In this study, an alternative view is proposed. Rather than using a dynamic friction model, a different approach focused on enhancing the system dynamics is explored, which can qualitatively lead to similar averaged friction results as the ones observed in the above-mentioned studies of Leus and Gutowski. In addition, instead of limiting the analysis to a single-degree-of-freedom system, the study incorporates the influence of longitudinal and transverse stiffnesses, offering a more comprehensive representation of the system's behaviour.

In this work, first, the system considered is presented. Then, a numerical analysis is performed to investigate the effect of longitudinal loading only on friction modulation. The numerical results are then compared to analytical ones obtained from a previous study [17], and a limitation of the latter is found for excitation frequencies approaching the resonance condition. To tackle this limitation, an enhanced expression for the velocity response amplitude at steady-state is proposed, highlighting the relevance of the additional friction-related damping at resonance. Afterwards, different transverse stiffness values are considered for the two-degree-of-freedom case, and their influence on vibration-assisted friction modulation under the effect of both longitudinal and transverse external loading is investigated. Lastly, a discussion relating the results of this study to those obtained using the Dahl and Dupont models is provided. Throughout this study, the contact is assumed to be in the sliding regime.

2. Description of the model and of the effective friction concept

2.1. Governing equation of the dynamic system

To reveal the effects of transverse stiffness on vibration-induced friction modulation, the system illustrated in Fig. 1 is considered. The system consists of an oscillator composed of a mass M positioned on a belt, moving at a constant speed V_b in the longitudinal direction X_1. In both directions, a linear spring and dashpot are present, with stiffnesses K_1 and K_2 and damping coefficients C_1 and C_2, in the longitudinal and transverse directions, respectively. Regarding the external load, both longitudinal and transverse loading, characterized by a frequency Ω_e and amplitude $mr\Omega_e^2$ (e.g., load arising from a horizontally unbalanced mass m at eccentricity r [11]), are applied as shown in Fig. 1.

For the chosen model setup, the kinetic friction is considered to be the same as the static friction. The adopted friction law is the Amontons-Coulomb's law [18,19], since the corresponding friction force is directly linked to a constant coefficient of friction, μ_s and proportional to the normal force. As the aim of this study is to capture the effect of transverse stiffness on vibration-induced friction modulation, the assumption of Amontons-Coulomb's law is deemed most appropriate, since it avoids the complexity of more realistic friction laws, which are case-study and material pair dependent [20,21]. The non-dimensional equations of motion of the system at non-dimensional time τ then become

$$\begin{bmatrix}1 & 0\\ 0 & 1\end{bmatrix}\begin{pmatrix}\ddot{x}_1\\ \ddot{x}_2\end{pmatrix}+\begin{bmatrix}2\beta_1 & 0\\ 0 & 2\beta_2\omega_r\end{bmatrix}\begin{pmatrix}\dot{x}_1\\ \dot{x}_2\end{pmatrix}+\begin{bmatrix}1 & 0\\ 0 & \omega_r^2\end{bmatrix}\begin{pmatrix}x_1\\ x_2\end{pmatrix} \tag{1}$$

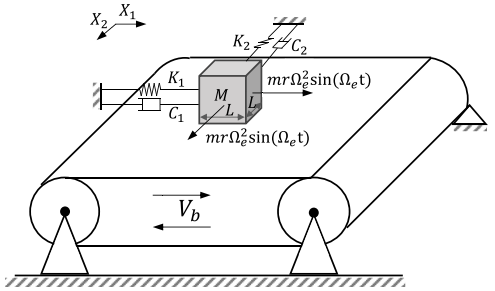

Fig. 1. Two-degree-of-freedom mass–spring-damper system sliding over a belt moving with constant velocity V_b.

$$+\begin{pmatrix}\frac{\mu_s\gamma^2(\dot{x}_1-v_b)}{\sqrt{(\dot{x}_1-v_b)^2+\dot{x}_2^2}}\\ \frac{\mu_s\gamma^2\dot{x}_2}{\sqrt{(\dot{x}_1-v_b)^2+\dot{x}_2^2}}\end{pmatrix}=\begin{pmatrix}\alpha\Omega^2\sin(\Omega\tau)\\ \alpha\Omega^2\sin(\Omega\tau)\end{pmatrix},$$

where

$$\tau=\omega_1 t,\quad x_1=\frac{X_1}{L},\quad x_2=\frac{X_2}{L},\quad \beta_1=\frac{C_1}{2M\omega_1},\quad \beta_2=\frac{C_2}{2M\omega_2},\quad \omega_1^2=\frac{K_1}{M},$$
$$\omega_2^2=\frac{K_2}{M},\quad \omega_r=\frac{\omega_2}{\omega_1},\quad \gamma^2=\frac{g/L}{K_1/M},\quad \Omega=\frac{\Omega_e}{\omega_1},\quad \alpha=\frac{mr}{ML},\quad v_b=\frac{V_b}{\omega_1 L}, \tag{2}$$

and the friction force is defined as follows:

$$\mathbf{F}_f=-\mu_s\gamma^2\frac{\mathbf{v}_r}{\|\mathbf{v}_r\|}=-\mu_s\gamma^2\frac{1}{\sqrt{(\dot{x}_1-v_b)^2+\dot{x}_2^2}}\begin{pmatrix}\dot{x}_1-v_b\\ \dot{x}_2\end{pmatrix}. \tag{3}$$

As shown from the equations of motion, this system consists of two nonlinear subsystems coupled through the friction force. It is important to note that the longitudinal and transverse excitation applied to the system have the same magnitude and frequency, with no phase shift between them. This type of loading can occur, for example, if an external force is applied at a 45-degree angle relative to the longitudinal direction of the mass. The effect of different loading phase shifts is not considered in the scope of this study.

2.2. Numerical validation of the analytical effective friction expression: case of longitudinal loading only

In this section, a numerical analysis is performed to obtain the average friction plots versus the belt velocity for the case of longitudinal loading only. This allows for a comparison with the approximated analytical results presented in a previous study [17], as the equations of motion in this work reduce to those of a single-degree-of-freedom (SDOF) system on a moving belt, which reads as follows

$$\ddot{x}_1+2\beta_1\dot{x}_1+x_1+\gamma^2\mu_s\mathrm{sgn}(\dot{x}_1-v_b)=\alpha\Omega^2\sin(\Omega\tau) \tag{4}$$

Before demonstrating the effect of vibration on friction modulation, it is important to define how the average friction is calculated. As described in [17], the average friction is evaluated by integrating (averaging) the time signature of the friction force over one oscillatory cycle driven by the excitation frequency. Note that, in the case of a SDOF system with loading in the longitudinal direction and with the friction force modelled using Amontons-Coulomb's law, the friction force depends on the sign of the relative velocity. Considering this approach, for the SDOF system described in [17], the equation of the average friction function for a harmonic excitation with arbitrary frequency is

$$\bar{\mu}(v_b)=\begin{cases}\mu_s\left(1-\frac{2}{\pi}\arccos\left(\frac{v_b}{\hat{V}}\right)\right) & \text{for } |v_b|\le\hat{V}\\ \mu_s\mathrm{sgn}(v_b) & \text{for } |v_b|\ge\hat{V},\end{cases} \tag{5}$$

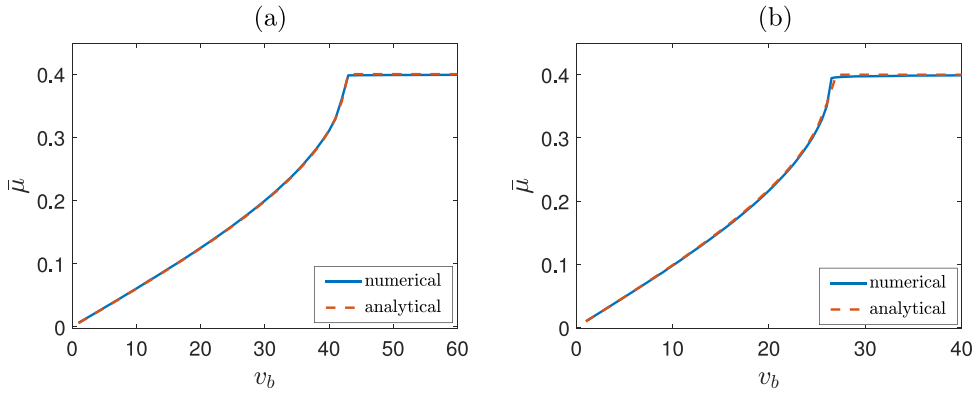

Fig. 2. Comparison of average friction results obtained numerically (blue line) and analytically (orange line): (a) excitation frequency in longitudinal direction $\Omega = 4$; (b) excitation frequency in longitudinal direction $\Omega = 2$. The rest of the parameters are $\beta_1 = 0.1$, $\mu_s = 0.4$, $\alpha = 10$ and $\gamma^2 = 1$.

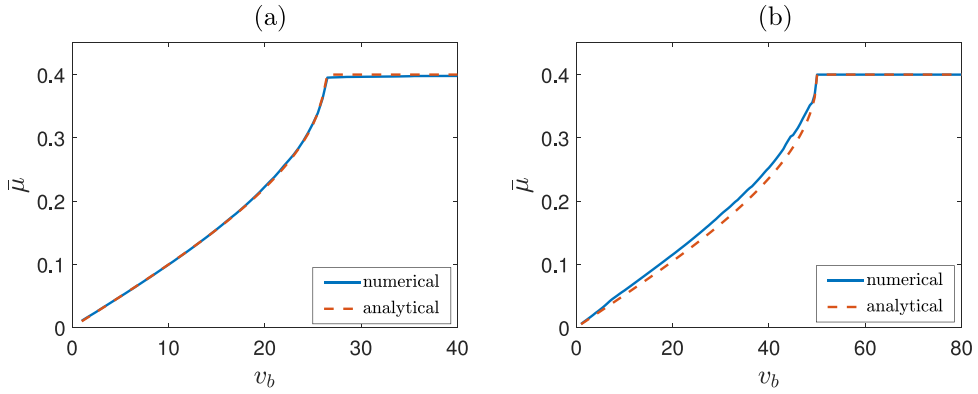

Fig. 3. Comparison of average friction results obtained numerically (blue line) and analytically (orange line) for $\gamma^2 = 1$: (a) excitation frequency in longitudinal direction $\Omega = 1.5$; (b) excitation frequency in longitudinal direction $\Omega = 1$. The rest of the parameters as in Fig. 2.

where $\hat{V}$ is the amplitude of the velocity response function at steady state (provided there is no stick–slip). In this section, the average friction values calculated numerically for the system in Fig. 1, with loading in the longitudinal direction only, are compared to those obtained analytically using Eq. (5), where $\hat{V}$ was

$$\hat{V}(\Omega) = \frac{\alpha\,\Omega^3}{\sqrt{(1-\Omega^2)^2 + \left(2\beta\Omega\right)^2}}. \tag{6}$$

The first comparisons for excitation frequencies $\Omega = 4$ and $\Omega = 2$ are shown in Fig. 2(a) and Fig. 2(b), respectively, which, as expected, portray very good matches between the numerical and analytical results. In Fig. 3(a) and Fig. 3(b), the same comparison is done for $\Omega = 1.5$ and $\Omega = 1$, respectively, with the latter matching the natural frequency of the undamped system in the X_1 direction. A very good agreement between the numerical and analytical results can also be observed for these excitation frequencies, with small discrepancies for the case of $\Omega = 1$. Using a higher value of γ^2, for example $\gamma^2 = 10$, leads to bigger discrepancies between the numerical and analytical results as shown in Fig. 4(a) and Fig. 4(b). The plots show that the agreement between numerical and analytical results deteriorates for $\Omega = 1.5$, particularly as v_b increases (except for v_b values where no friction variation is observed); however, the discrepancies are moderate. In contrast, for $\Omega = 1$, the differences between numerical and analytical results are considerably large across all v_b values (apart from the cases where no friction variation occurs).

As previously noted, the use of the analytical technique based on the Method of Direct Separation of Motion adopted in [17], was meant to obtain a closed-form solution of the velocity-response amplitude ($\hat{V}$), Eq. (6), that resulted to be independent of the friction force and, therefore, of the relative velocity (which depends on the belt velocity v_b). In order to do so, the solution for the fast motion was assumed to be decoupled from the solution of the slow motion. Such assumption seems to be good enough for $\gamma^2 = 1$, where the friction force is relatively weak and the numerical results closely match the analytical ones, indicating that the friction force caused by sliding has little influence on the velocity response, as shown in Fig. 5(a). In contrast, for the same excitation frequency $\Omega = 1$ and $\gamma^2 = 10$ (higher friction force), Fig. 5(b) shows that the numerically obtained velocity responses depend significantly on the belt velocity, leading to larger discrepancies between the numerical and analytical average friction values, as shown in Fig. 4(b).

Therefore, it is important to note that the analytical results for the average friction expression, derived in [17], match with the numerical ones at any excitation frequency when the friction force is weak in

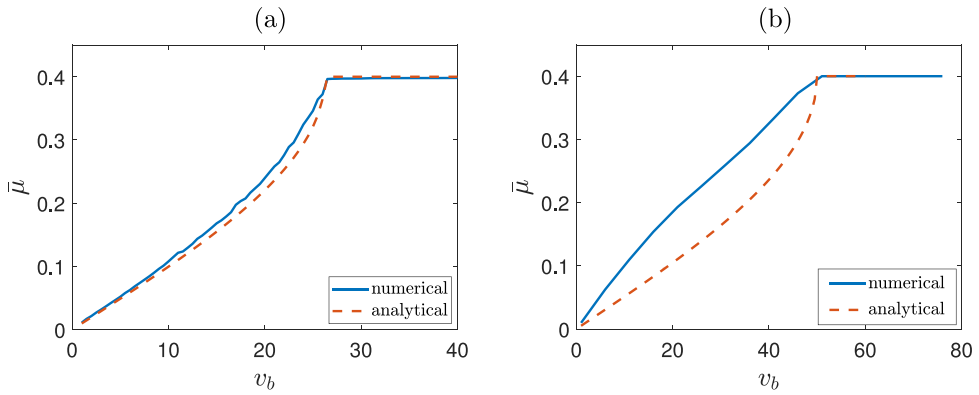

Fig. 4. Comparison of average friction results obtained numerically (blue line) and analytically (orange line) $\gamma^2 = 10$: (a) excitation frequency in longitudinal direction $\Omega = 1.5$; (b) excitation frequency in longitudinal direction $\Omega = 1$. The rest of the parameters as in Fig. 2.

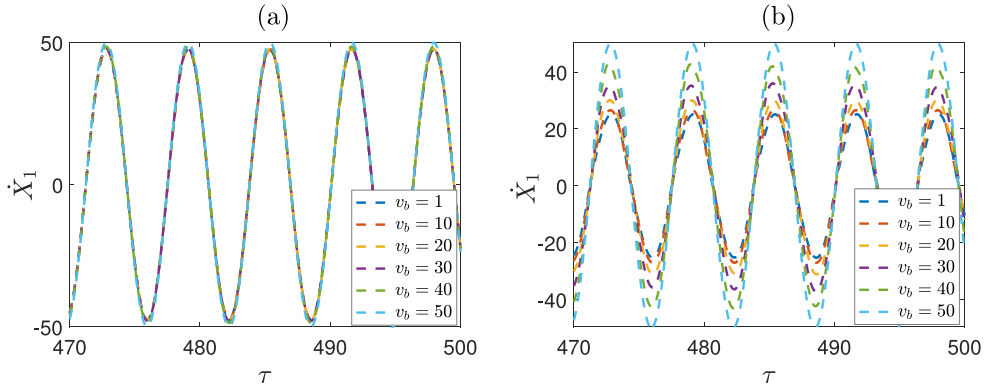

Fig. 5. Steady-state velocity response in longitudinal direction for different v_b values: (a) $\Omega = 1$ and $\gamma^2 = 1$; (b) $\Omega = 1$ and $\gamma^2 = 10$. The rest of the parameters are as in Fig. 2.

comparison to the viscous damping term. However, for stronger friction forces, discrepancies between analytical and numerical results appear, specifically near and at resonance.

Fig. 6 illustrates a comparison of the dimensionless energies dissipated by viscous damping, $E_{dis,v}$, and friction damping, $E_{dis,f}$, calculated as follows:

$$E_{dis,v} = \int 2\beta_1 \dot{x}_1^2 \mathrm{d}\tau, \qquad E_{dis,f} = \int \gamma^2 \mu_s \mathrm{sign}(\dot{x}_1 - v_b)\dot{x}_1 \mathrm{d}\tau \tag{7}$$

The comparison is shown for two values of $\gamma^2 = 1$ and $\gamma^2 = 10$ with $\Omega = 1$ for both cases. Fig. 6(a), corresponding to $\gamma^2 = 1$, shows that the energy dissipated by viscous damping is at least around 20 times bigger than that dissipated by the friction force. The difference becomes bigger for increasing v_b values with $E_{dis,v}$ increasing and $E_{dis,f}$ approaching zero. Moreover, the variation in the dissipated energy values with respect to v_b remains relatively small for both cases, which aligns with the observation that the velocity responses are similar across the range of v_b values. Thus, for this value of γ, the contribution of frictional damping is negligible compared to that of viscous damping, and the influence of the friction force on the amplitude of the velocity response at resonance in X_1 direction is minimal. In contrast, Fig. 6(b), which corresponds to $\gamma^2 = 10$, shows that the energies dissipated by viscous and friction damping are more comparable, especially at low v_b values, even though the difference between the two forms of energy dissipation increases as v_b increases. This indicates that the influence of friction damping is stronger at higher γ values and for belt velocities lower than 50. Therefore, the numerical results that take into account this contribution differ more significantly from analytical solutions that neglect this effect.

An attempt is made to update the closed-form expression for the velocity response used in [17]. The complete derivation of this is provided in Appendix, and the final implicit expression of the velocity response, including a friction-related term $F(\hat{V})$, is shown below

$$\hat{V}(\Omega) = \frac{\alpha\, \Omega^3}{\sqrt{(1-\Omega^2)^2 + \left(2\beta\Omega + F(\hat{V})\right)^2}}, \tag{8}$$

in which $F(\hat{V})$ depends on the occurrence of the sign flip and is defined by

$$F(\hat{V}) = \begin{cases} \dfrac{4\gamma^2 \mu_s\, \Omega}{\pi \hat{V}} \sqrt{1 - \left(\dfrac{v_b}{\hat{V}}\right)^2}, & \hat{V} > |v_b| \quad \text{(sign flip)}, \\ 0, & \hat{V} \le |v_b| \quad \text{(no sign flip)}. \end{cases} \tag{9}$$

It is important to note that Eq. (8) is implicit and requires a numerical solver (a bisection method was used here). However, it still enables us to gain further physical insights on how the velocity response behaves as a function of external parameters. For example, as mentioned before, for small values of γ, $F(\hat{V})$ tends to become smaller, hence its influence on the velocity response decreases accordingly. In addition, depending on the ratio between $\hat{V}$ and v_b, the following cases occur:

- As $|v_b| \to \hat{V}$, $F \to 0$ and Eq. (8) becomes Eq. (6) (the latter corresponding to the expression used in [17]).
- As $v_b \to 0$, $F(\hat{V}) \to \dfrac{4\gamma^2 \mu_s\, \Omega}{\pi \hat{V}}$ (which corresponds to the case characterized by an equivalent viscous damping of Coulomb friction).

It is worth mentioning the reason why $F(\hat{V})$ becomes zero for the case in which no sign flip occurs. According to the derivation and notation shown in Appendix, if $|v_b| \ge \hat{V}$, then $\dot{x} - v_b = \hat{V}\cos\theta - v_b$ never

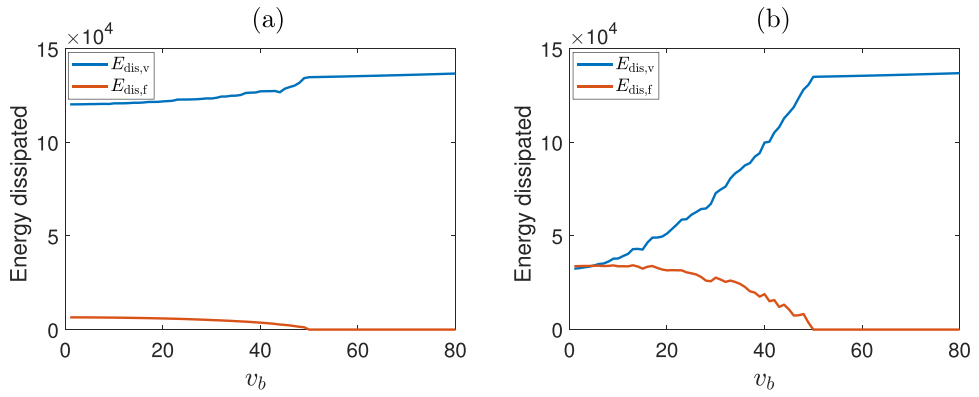

Fig. 6. Energies dissipated by viscous and friction damping for $\Omega = 1$: (a) $\gamma^2 = 1$; (b) $\gamma^2 = 10$. The rest of the parameters are as in Fig. 2.

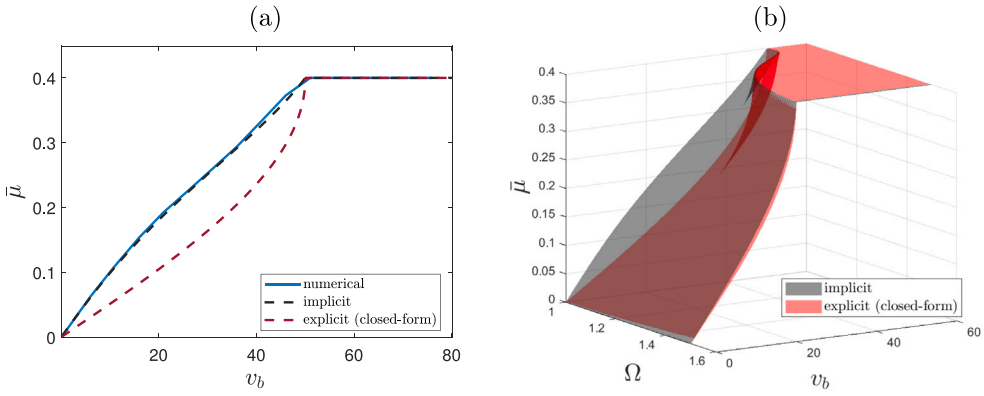

Fig. 7. Comparison of average friction for $\gamma^2 = 10$. The black curve shows the numerical results obtained using the implicit expression in Eq. (8), the red curve represents the closed-form analytical solution, and the blue line corresponds to the numerical results from Fig. 4(b). The rest of the parameters as in Fig. 2: (a) longitudinal excitation frequency of $\Omega = 1$, (b) varying longitudinal excitation frequency, $\Omega \in [1, 1.5]$.

changes sign over the period, so $\mathrm{sign}(\hat{V}\cos\theta - v_b) = \pm 1$ is a constant term. Its fundamental cosine coefficient is

$$b_1 = \frac{1}{\pi}\int_0^{2\pi} (\pm 1)\cos\theta \, d\theta = 0 \quad \Longrightarrow \quad F(\hat{V}) = 0 \text{ when } |v_b| \geq \hat{V}. \tag{10}$$

Physically, the DC part $c_0 = \pm 1$ remains and enforces a static offset $\bar{x} = -\gamma^2 \mu_s c_0$, but it does not get projected into the fundamental cosine term of the friction function, Eq. (A.9). The results discussed previously in Fig. 6, confirm that as soon as no sign flip occurs ($|v_b| \geq \hat{V}$), the dissipated energy by "Coulomb-like" friction damping is zero, hence $F(\hat{V})$ becomes uninfluential.

In the case of a sign flip, which leads to friction modulation, the DC term (c_0) of the Fourier series has its own relevance, since it corresponds to the averaged friction expression derived by applying the method of direct separation of motion as in [17]. Specifically, as a result of the Harmonic Balance technique (see Appendix), the mean (DC) shift is

$$\bar{x} = -\gamma^2 \mu_s \, c_0 = -\gamma^2 \mu_s \left(\frac{2}{\pi}\arccos\kappa - 1\right) \tag{11}$$

in which $\bar{x}$ balances the drifted friction force, according to DC balance shown in Eq. (A.17).

Fig. 7(a) shows the result of using the updated velocity response expression (Eq. (8), see black line) in comparison with the closed-form expression (Eq. (6), see red line). The parameters used are listed in the caption of Fig. 2. The result obtained for the resonance case resembles the result obtained numerically (blue line). Fig. 7(b) provides a 3D view on how the effective friction curve changes as soon the excitation frequency increases with respect to the natural frequency. As Ω increases, the red and the blue surfaces tend to touch and match each other. At $\Omega = 1.5$ the result resembles the one shown in Fig. 4(a). It is worth highlighting that the comparison between the implicit and explicit expressions also depends on the viscous damping value assumed in this analysis, and in general on the interplay concerning the dominance between viscous and friction damping.

2.3. A note on the system's internal resonance

Lastly, by assuming the application of only a longitudinal loading, the equations of motion were reduced to that of a single-degree-of-freedom system, neglecting any eventual vibratory response along the X_2 direction. While this may hold true for most of the parameter space, the presence of the nonlinear coupling through the friction force between the two directions implies that the system can still exhibit oscillations along the X_2 direction, even when the excitation is applied in the X_1 direction only. This phenomenon can occur if the system exhibits internal resonance, for example, when the ratio of natural frequencies is 1:2 ($\omega_r = 0.5$). For this case, it can be shown that multimodal solutions (responses in both X_1 and X_2 directions) are often unstable [22,23]. Even when they do exist and are stable, numerical simulations should be approached with caution, as they are sensitive to initial conditions and the basin of attraction may be small. Furthermore, it can be verified that when oscillations in the X_2 direction occur, their amplitudes are very small. Although these oscillations are small in amplitude, the coupling in the system leads to significant changes in the main response in the X_1 direction. Since the response in X_1 direction is affected by the presence of internal resonance, this in turn changes the averaged friction curve. However, a parametric analysis of the internal resonances and their exact effect on friction modulation is beyond the scope of this study.

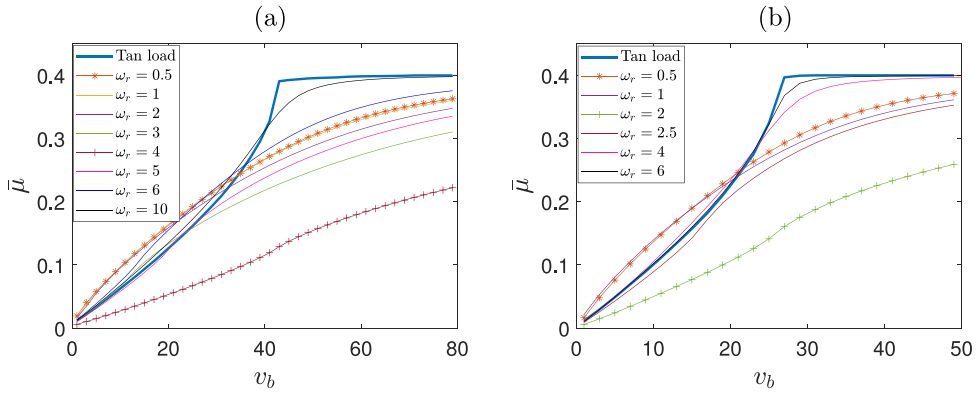

Fig. 8. Average friction plots for different ω_r values: (a) $\Omega = 4$; (b) $\Omega = 2$. $\beta_2 = 0.1$ and the rest of the parameters as in Fig. 2.

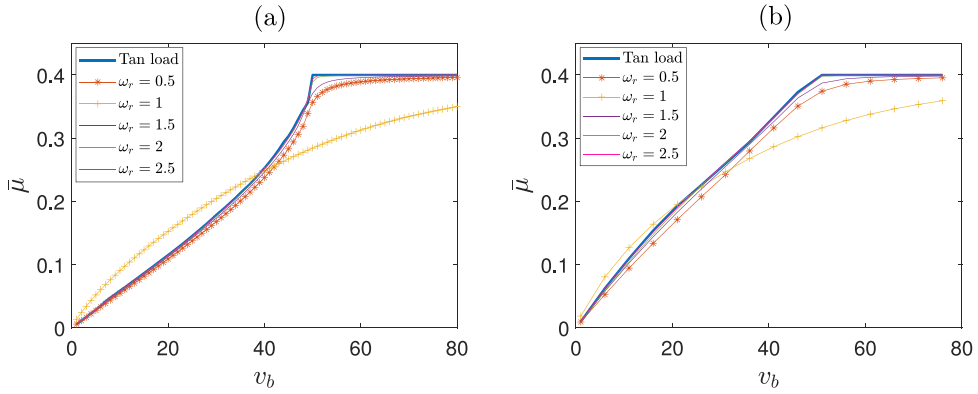

Fig. 9. Average friction plots for $\Omega = 1$ and for different ω_r values: (a) $\gamma^2 = 1$; (b) $\gamma^2 = 10$. The rest of the parameters as in Fig. 2.

3. Transverse stiffness effect on friction modulation: longitudinal and transverse loading

In this section, loading acting in both transverse and longitudinal directions is considered. For different excitation frequencies, the effect of transverse stiffness on the average friction values is investigated by varying the ratio of transverse to longitudinal natural frequency ω_r. It should be noted that the reported average friction values correspond to changes in the longitudinal friction force, so in the component of the friction force along the X_1 direction.

First, as done in the previous section, the excitation frequency $\Omega = 4$ is considered. The results are reported in Fig. 8(a), with the blue line referring to the longitudinal-only loading case, which serves as a reference, indicating the average friction behaviour without the influence of the transverse stiffness. The other curves are obtained using loadings in both directions with ω_r values varying from 0.5 ($\omega_2 < \omega_1$) to 4 ($\omega_2 = \Omega_e$) and lastly 10 ($\omega_2 > \omega_1$ and $\omega_2 > \Omega$). For low ω_r values (e.g. $\omega_r = 0.5$, marked with * for a better distinction from other closely present curves), and low V_b values (< 35), the average friction values are higher than those for higher ω_r values and longitudinal loading only. At higher belt velocities, the presence of transverse loading leads to a higher reduction of the averaged friction, than longitudinal loading only, independent of the transverse stiffness values. As the value of the latter increases, the average friction values decrease, reaching their minimum for $\omega_r = 4$, which corresponds to the excitation frequency. Thus, the reduction is the biggest at resonance in the X_2 direction. Then, as the ω_r value increases further, the average friction values increase again, approaching the longitudinal loading cases as shown, for example, for $\omega_2 = 10$.

Not only the values, but also the shape of the average friction plots vary depending on ω_r. For low ω_r values, different from the longitudinal-only case, the curves have a concave shape. This shape has also been observed in other studies that consider the effect of transverse loading on friction reduction [8–10,15], where no transverse stiffness was considered. As the ω_2 increases, the curve gradually transitions to a convex shape. More specifically, for transverse stiffness values corresponding to the excitation frequency, the average friction curve is partially convex and partially concave. As ω_r increases further, the curves approach the longitudinal-only curve shape but do not exhibit the characteristic kink. Instead, they transition more smoothly, indicating a gradual variation in the average friction values. In Fig. 8(b), the same plots are obtained for a lower excitation frequency, $\Omega = 2$, showing the same trends in terms of values and shapes as in Fig. 8(a). Again, for low ω_r and low v_b values, the average friction values are higher than those for high ω_r values. The average friction values reach their minimum for $\omega_r = 2$, which corresponds to the excitation frequency (resonance in the X_2 direction) and increase for increasing ω_r, approaching the longitudinal loading cases.

Lastly, Fig. 9 presents the results for $\Omega = 1$, which corresponds to the natural frequency ω_1, with Fig. 9(a) and Fig. 9(b) corresponding to results for $\gamma^2 = 1$ and $\gamma^2 = 10$, respectively. In this loading scenario, variations in ω_r lead to smaller changes in the average friction values compared to other excitation frequency cases. Specifically, for $\gamma^2 = 1$, when $\omega_r = \Omega = 1$, ($\Omega_e = \omega_2$ and, differently from before, $\Omega_e = \omega_1$

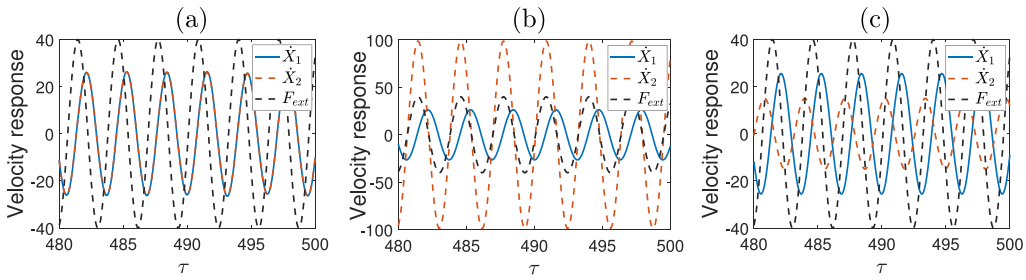

Fig. 10. Relative velocity plots and external excitation for $\Omega = 2$: (a) $\omega_r = 1$ and velocity responses are in phase; (b) $\omega_r = 2$ and velocity responses are 90° out of phase; (c) $\omega_r = 3$ and velocity responses are 180° out of phase. The rest of the parameters as in Fig. 2.

too, so, resonance in both directions) the average friction curve is no longer the lowest at all v_b values, marking another difference from the behaviour observed at other excitation frequencies, see Fig. 9(a). For all the other ω_r values, the plots of average friction are close to each other and to the longitudinal-only loading case. As the system is now resonating in the X_1 direction, the influence of the response in the X_2 direction is lower than before and the average friction results are closer to the longitudinal-only loading case. Moreover, as shown in Fig. 9(b), for $\gamma^2 = 10$, less friction reduction (compared to $\gamma^2 = 1$) is observed for all ω_r values. This outcome is attributed to lower velocity response amplitude values that occur in this scenario, as shown in Fig. 5(b). It is important to highlight that, in this case, the average friction curve exhibits a concave shape even when longitudinal-only loading is applied. Thus, when the mass is excited at resonance along the X_1 direction and the friction damping is dominant, the system exhibits both less friction reduction, compared to the weak friction case, and a concave average friction curve, even under longitudinal excitation only.

To better understand the difference in the average friction curve trends between the case of $\Omega = 1$ and other excitation frequencies, Fig. 10 and Fig. 11 are plotted. These figures illustrate the velocity responses for $\Omega = 2$ and $\Omega = 1$, respectively, considering for each case three ω_r values: below, at, and above resonance. For $\Omega = 2$ and $\omega_r = 1$, Fig. 10(a) shows the velocity responses along the X_1 and X_2 directions to be in phase with each other and 90° out of phase with the external load F_{ext}. It should be noted that the phase shift analysis presented here is with respect to the velocity response, not the displacement response and the observations in terms of amplitude and phase are in accordance with the linear theory of vibration (as the velocity response is in phase with the excitation at resonance and approximately 90° out of phase elsewhere). As shown in Fig. 8(b), this configuration corresponds to the highest average friction values (at low belt velocities). At resonance along the X_2 direction, so for $\omega_r = 2$, Fig. 10(b) shows the responses $\dot{x}_1$ and $\dot{x}_2$ to be 90° out of phase. With respect to the external force, $\dot{x}_2$ is in phase, while $\dot{x}_1$ is 90° out of phase. This case results in the lowest average friction, as shown in Fig. 8(b). For $\omega_r = 3$, Fig. 10(c) shows the responses $\dot{x}_1$ and $\dot{x}_2$ to be 180° out of phase. Both responses are approximately 90° out of phase with the external force. In this case, the average friction increases again and tends to converge towards the values observed under purely longitudinal excitation. These observations indicate that the highest average friction occurs when the velocity responses are in phase with each other and out of phase with the external force (e.g., for $\omega_r = 1$), while the lowest average friction is obtained when the responses are 90° out of phase with each other and $\dot{x}_2$ is in phase with the external force. This conclusion holds for higher excitation frequencies as well.

As shown in Fig. 11b, for the case of $\Omega = 1$, the velocity responses are in phase for $\omega_r = 1$. As established in the previous paragraph, this phase relationship leads to the highest average friction values at low belt velocities, which is indeed the case, as shown in Fig. 9(a). The other two cases show responses to be 90° out of phase with each other and, with respect to the external force, $\dot{x}_1$ is in phase, while $\dot{x}_2$ is 90° out of phase, similar to the resonance case in Fig. 10(b). This configuration leads to lower average friction values, even though, as already mentioned, the variations from the longitudinal-only case are small.

4. Discussion and comparison with the Dahl-like friction model

Lastly, a discussion is provided between the findings obtained in this study and related experimental works. Several researchers have developed and studied models to investigate the phenomenon of friction force reduction under the effect of loading in longitudinal, transverse or both directions and compared the results to those obtained in experimental campaigns. These studies have generally shown that much better compliance with experimental results is obtained when, instead of the Amonton-Coulomb law, dynamic friction models such as Dahl and Dupont were considered. These models account for contact compliance, so they assume that the friction force depends on the elastic deflection, and corresponding memory effect, of the contact zone in the slip direction.

More specifically, Kapelke employed the Dupont model and the Amontons-Coulomb law to compare the experimental results to theoretical ones [24]. The experimental results showed an excellent match to the elasto-plastic Dupont model, for moderate excitation frequencies; however, when high-excitation frequencies were used to catch the behaviour of the friction force accurately, a significantly different value of tangential stiffness was needed for the Dupont model. Gutowski and Leus also developed a model to investigate how a harmonic excitation applied along arbitrary directions affect the friction force [16]. To capture the resultant modulated friction force, dynamic friction models such as the Dahl and Dupont model were adopted, and assumptions were made regarding the rate of change of elastic deformation of the contact, which depends, among other parameters, on the contact stiffness in the longitudinal direction. The results of the numerical analysis carried out using the developed models showed very good consistency with the outcomes of the experimental tests for the cases considered in the study.

In the referenced studies, the use of dynamic friction models resulted in average friction curves exhibiting a concave shape. In the present study, a similar concave shape is observed in two cases, one of which occurs when the excitation frequencies are close to or at resonance, as shown in Fig. 4(b), under longitudinal loading at and nearby resonance conditions (no transverse stiffness/vibration and high γ^2 is required). This highlights the importance of accounting for the system dynamics and eventual resonant conditions. As shown later in Fig. 9, for the same excitation frequency (at resonance in X_1 direction), variations in transverse stiffness values have small influence on the resulting average friction plots. The other case in which concave average friction shapes are observed occurs when loading in both directions and low transverse stiffness values are employed, even though the Amonton-Coulomb's law is used, as shown in Fig. 8. Thus, the concave shape does not arise exclusively from the use of dynamic friction models but can also result from the presence of transverse stiffness or from

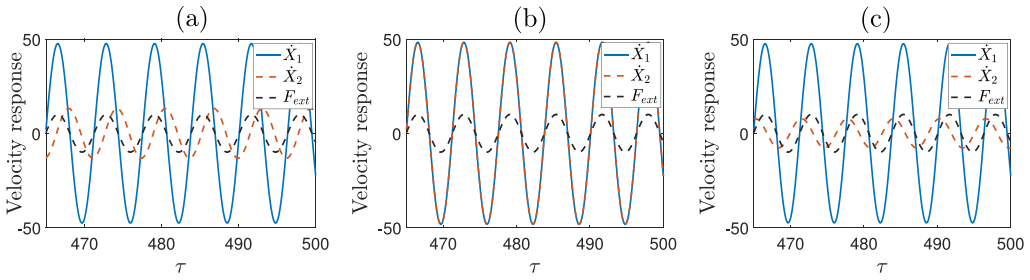

Fig. 11. Relative velocity plots and external excitation for $\Omega = 1$: (a) $\omega_r = 0.5$ and velocity responses are 90° out of phase; (b) $\omega_r = 1$ and velocity responses are in phase; (c) $\omega_r = 1.5$ and velocity responses are 90° out of phase. The rest of the parameters as in Fig. 2.

resonance occurring in the longitudinal direction (be it a "system" or "contact" resonance condition). However, in terms of friction reduction, the findings of Kapelke and Gutowski and Leus demonstrated that Amonton-Coulomb's law tends to overestimate the reduction in friction due to vibrations, leading to predictions that deviate from experimental results. Similarly, in our study, higher average friction values were observed for low transverse stiffness values. The discrepancies in friction reduction between the cases with and without transverse stiffness were less pronounced than those reported in the works of Kapelke and Gutowski and Leus.

These discrepancies indicate that the "true" behaviour of the average friction under an external excitation is probably somewhere in between these modelling approaches. Models such as those of Dahl and Dupont incorporate contact compliance into the friction formulation itself, and as a result, are capable of describing complex behaviours, but may lack generality as their parameters often require tuning based on the excitation frequency and cannot always be directly linked to material properties. Alternatively, using the more simplistic Amonton-Coulomb's law and considering the transverse stiffness as a system parameter allows getting a clearer picture of the role of the system stiffness in friction modulation. It should be noted that while our model exhibits similar apparent phenomena in terms of the concave shape of the average friction curve as seen in the Dahl and Dupont models, these approaches are not mathematically isomorphic. Microscopic models like Dahl or Dupont incorporate a contact compliance and also a contact damping directly into the friction formulation, and the link between the two is governed by an ad-hoc state evolution law which defines an "inner interface dynamics". Because of the presence of contact compliance and contact damping, any equivalent friction damping model meant to approximate such "dynamic friction model" through the Harmonic Balance method, will be characterized by an in-phase and also an out-of-phase term (contact stiffness and contact damping are in quadrature between each other), which will look different from the $F(\hat{V})$ term derived in this work (see Eq. (9)). Previous studies, such as the works of Cabboi and Woodhouse [20,21], have already pointed out that a linearized form (formulated in the frequency domain) of such dynamic friction models (the Dieterich-Ruina dynamic friction law was used in their studies), leads to a complex impedance function, which again differs fundamentally from the equivalent Coulomb damping.

It is worth mentioning that similar averaged effects caused by dynamic interface models such as the Dahl and Dupont, could also be obtained by "equivalent" nonlinear viscoelastic damping models or fractional viscoelastic models (see [25–27]). However, the effect of such nonlinear damping models were not investigated in the current framework, but they may provide further insights on the observed dissipation mechanism occurring under external excitation. Ultimately, neither approach alone fully captures the multi-dimensional character of frictional behaviour under external excitation. A more comprehensive understanding may be achieved by combining these perspectives whenever comparisons with experimental data are carried out, to provide more robust and generalizable insights into friction modulation under different excitation conditions.

5. Conclusions

This work investigates the influence of transverse stiffness and resonance condition on the modulation of friction in a two-degree-of-freedom system subjected to longitudinal and transverse loading. Initially, the case with longitudinal loading only is considered, and numerical results for average friction are compared with analytical predictions obtained using the extended MDSM. The average friction results from both approaches match for any excitation frequency when the friction force is weak. However, for stronger friction forces, discrepancies between analytical and numerical results appear, specifically near and at resonance, with the results from the extended MDSM overestimating friction reduction. This discrepancy arises due to the damping effect of friction that is mostly pronounced in the damping-dominated region, an effect not captured by the assumptions made while adopting the extended MDSM. In order to capture the additional friction-related damping, an enhanced implicit expression for the velocity response amplitude at steady-state is provided, showing an excellent agreement with the numerical results.

Then, the effect of transverse stiffness is analysed under combined longitudinal and transverse loading. The average friction plots reveal that, for transverse stiffness values smaller than the excitation frequencies and at low belt velocities, the average friction values are higher than the reference case of longitudinal loading only. As the transverse stiffness increases, friction reduction becomes more pronounced, reaching a minimum at resonance in X_2 direction ($\omega_r = \Omega$). Thus, the influence of the transverse motion on the average friction is most significant when resonance occurs in the X_2 direction. However, this influence is less pronounced if resonance occurs in the X_1 direction as well. For higher transverse stiffness values, the average friction curves approach the longitudinal-only loading case. The average friction plots also exhibit a concave shape under certain parameter values and loading conditions. More specifically, the concave shape is observed when the excitation frequency is near or at resonance (longitudinal-only loading and strong friction force). For loading in both directions and higher excitation frequencies, the concave shape arises for low transverse stiffness values. In both these cases, Amonton-Coulomb's friction law is used, indicating that the concave shape is not exclusively a result of employing dynamic friction models, as shown in other related studies. These results highlight the importance of properly accounting for the system dynamics in studies aimed at identifying friction change.

CRediT authorship contribution statement

E. Sulollari: Writing – review & editing, Writing – original draft, Visualization, Validation, Software, Methodology, Investigation, Formal

analysis, Data curation, Conceptualization. **K.N. van Dalen:** Writing – review & editing, Supervision. **A. Cabboi:** Writing – review & editing, Writing – original draft, Visualization, Supervision, Methodology, Investigation, Formal analysis, Data curation, Conceptualization.

Declaration of competing interest

The authors declare that they have no known competing financial interests or personal relationships that could have appeared to influence the work reported in this paper.

Appendix. Harmonic-balance derivation of the velocity response for an SDOF sliding over a moving belt

The steady-state response of the system

$$\ddot{x} + 2\beta\dot{x} + x + \gamma^2\mu_s \operatorname{sgn}\big(\dot{x} - v_b\big) = \alpha\Omega^2 \sin(\Omega\tau), \tag{A.1}$$

is considered, where $\beta, \gamma, \mu_s, \alpha, v_b$ are constants, Ω is the excitation frequency, and τ denotes the dimensionless time (see also [17] for details on the nondimensional parameters). The objective is to derive the velocity response amplitude in the frequency domain, $\hat{V}(\Omega)$, using a first-order harmonic balance (HB) approximation.

The following harmonic ansatz is considered

$$x(\tau) = X_s \sin\Omega\tau + X_c \cos\Omega\tau + \bar{x}, \qquad \dot{x}(\tau) = \Omega\big(X_s \cos\Omega\tau - X_c \sin\Omega\tau\big), \tag{A.2}$$

and the fundamental displacement amplitude is defined as $R = \sqrt{X_s^2 + X_c^2}$, with the velocity amplitude $\hat{V} = \Omega R$, and the phase angle ψ

$$\cos\psi = \frac{X_s}{R}, \qquad \sin\psi = -\frac{X_c}{R}. \tag{A.3}$$

With these definitions, the velocity is expressed as

$$\dot{x}(\tau) = \Omega R \cos(\Omega\tau - \psi) = \hat{V}\cos(\Omega\tau - \psi), \tag{A.4}$$

where the following trigonometric identity is employed

$$\cos(\Omega\tau - \psi) = \cos(\Omega\tau)\cos(\psi) + \sin(\Omega\tau)\sin(\psi). \tag{A.5}$$

The friction force function can be approximated through the Fourier content of the biased (due to v_b) signum function. For simplification, let us introduce $\theta = \Omega\tau - \psi$, so as to express an arbitrary friction function with respect to the relative velocity sign

$$f(\theta) = \operatorname{sgn}\big(\hat{V}\cos\theta - v_b\big) = \operatorname{sgn}\big(\cos\theta - \kappa\big), \qquad \text{and} \qquad \kappa = \frac{v_b}{\hat{V}}. \tag{A.6}$$

When $|\kappa| < 1$, indicating that the velocity response amplitude is bigger than v_b, the sign flips in each cycle. The instances at which the sign reversal occurs are determined by solving for κ

$$\cos\theta = \kappa \qquad \text{hence} \qquad \theta = \arccos\kappa. \tag{A.7}$$

Within a single period, the solutions are given by

$$\theta_0 = \arccos\kappa \in [0, \pi], \qquad \text{and} \qquad \theta_1 = 2\pi - \theta_0. \tag{A.8}$$

The intervals over which f is constant are identified as follows :

- $f(\theta) = +1$ when $\cos\theta > \kappa$, i.e. for $\theta \in (-\theta_0, \theta_0)$ which repeats every 2π;
- $f(\theta) = -1$ on the complement, i.e. for $\theta \in (\theta_0, 2\pi - \theta_0)$ which repeats every 2π;.

Equivalently, in piecewise form,

$$f(\theta) = \begin{cases} +1, & \theta \in (-\theta_0, \theta_0) \bmod 2\pi, \\ -1, & \theta \in (\theta_0, 2\pi - \theta_0) \bmod 2\pi. \end{cases}$$

It should be noted that if $|\kappa| \geq 1$, $f(\theta)$ remains constant over the entire period with $f = -1$ for $\kappa \geq 1$ and $f = +1$ for $\kappa \leq -1$. For $|\kappa| < 1$, since f is an even function, its Fourier series contains only cosine terms. Keeping the DC term and the first harmonic, the function can be approximated as

$$f(\theta) \approx c_0 + b_1 \cos\theta, \tag{A.9}$$

with coefficients

$$c_0 = \frac{1}{2\pi}\int_0^{2\pi} f(\theta)\, d\theta = \frac{(+1)\cdot 2\theta_0 + (-1)\cdot(2\pi - 2\theta_0)}{2\pi} = \frac{2}{\pi}\theta_0 - 1 = \frac{2}{\pi}\arccos\kappa - 1\,, \tag{A.10}$$

$$b_1 = \frac{1}{\pi}\left(\int_0^{\theta_0}\cos\theta\, d\theta + \int_{2\pi-\theta_0}^{2\pi}\cos\theta\, d\theta - \int_{\theta_0}^{2\pi-\theta_0}\cos\theta\, d\theta\right) \tag{A.11}$$

$$= \frac{1}{\pi}\Big(\sin\theta_0 + \big[\sin 2\pi - \sin(2\pi - \theta_0)\big] - \big[\sin(2\pi - \theta_0) - \sin\theta_0\big]\Big) \tag{A.12}$$

$$= \frac{1}{\pi}\Big(\sin\theta_0 + \sin\theta_0 - (-\sin\theta_0) - \sin\theta_0\Big) \tag{A.13}$$

$$= \frac{4}{\pi}\sin\theta_0 = \frac{4}{\pi}\sqrt{1-\kappa^2}. \tag{A.14}$$

As mentioned earlier, in case $|\kappa| \geq 1$, the function f is constant, with $b_1 = 0$ and $c_0 = \pm 1$, where $c_0 = +1$ for $\kappa = -1$ and $c_0 = -1$ for $\kappa = +1$. Note that the approximated decomposition of the friction force into a DC term and a first harmonic term, as highlighted in Eq. (A.9), resembles the assumption of slow (DC term) and fast motion (harmonic term) made by the Method of Direct Separation of Motion described in a previous study [17].

Mapping back to time to Eq. (A.4) and using the trigonometric identity

$$\cos(\Omega\tau - \psi) = \frac{X_s}{R}\cos\Omega\tau - \frac{X_c}{R}\sin\Omega\tau, \tag{A.15}$$

the first order harmonic approximation of the friction nonlinearity is obtained

$$\operatorname{sgn}\big(\dot{x} - v_b\big) \approx c_0 + b_1\left(\frac{X_s}{R}\cos\Omega\tau - \frac{X_c}{R}\sin\Omega\tau\right). \tag{A.16}$$

The harmonic ansatz $x(\tau)$ from Eq. (A.2), along with its time derivatives and the first-order harmonic approximation of the friction function from Eq. (A.16), are substituted into the equation of motion (Eq. (A.1)). The resulting expression is then decomposed by matching the DC, $\sin\Omega\tau$, and $\cos\Omega\tau$ coefficients, leading to

$$\bar{x} + \gamma^2\mu_s c_0 = 0 \quad \Rightarrow \quad \bar{x} = -\gamma^2\mu_s c_0. \tag{A.17}$$

To balance out the first harmonic terms, we define $A = 1 - \Omega^2$, $a = 2\beta\Omega$ and the (amplitude-dependent) coupling

$$F = \frac{\gamma^2\mu_s\, b_1}{R} = \frac{4\,\gamma^2\mu_s}{\pi R}\sqrt{1 - \left(\frac{v_b}{\hat{V}}\right)^2}, \qquad (\hat{V} = \Omega R > |v_b|;\ \text{otherwise } F = 0). \tag{A.18}$$

The equations corresponding to the sine and cosine components are then given by

$$A X_s - a X_c - F X_c = \alpha\Omega^2, \tag{A.19}$$

$$a X_s + A X_c + F X_s = 0. \tag{A.20}$$

In matrix form, these can be expressed as

$$\begin{bmatrix} A & -a - F \\ a + F & A \end{bmatrix}\begin{bmatrix} X_s \\ X_c \end{bmatrix} = \begin{bmatrix} \alpha\Omega^2 \\ 0 \end{bmatrix}. \tag{A.21}$$

The determinant of the coefficient matrix is

$$D = A^2 + (a + F)^2, \tag{A.22}$$

from which the solutions for X_s and X_c are

$$X_s = \frac{\alpha\Omega^2 A}{D}, \qquad X_c = -\frac{\alpha\Omega^2 (a + F)}{D}. \tag{A.23}$$

Consequently, the response amplitude R and the velocity amplitude $\hat{V}$ are

$$R = \sqrt{X_s^2 + X_c^2} = \frac{\alpha\Omega^2}{\sqrt{A^2 + (a+F)^2}}, \tag{A.24}$$

$$\hat{V}(\Omega) = \Omega R = \frac{\alpha\,\Omega^3}{\sqrt{(1-\Omega^2)^2 + \left(2\beta\Omega + F(\hat{V})\right)^2}}. \tag{A.25}$$

The expression $F = F(\hat{V})$ follows from Eq. (A.18) and $R = V/\Omega$:

$$F(\hat{V}) = \begin{cases} \dfrac{4\,\gamma^2\mu_s\,\Omega}{\pi\hat{V}}\sqrt{1-\left(\dfrac{v_b}{\hat{V}}\right)^2}, & \hat{V} > |v_b| \quad \text{(sign flip)}, \\ 0, & \hat{V} \le |v_b| \quad \text{(no sign flip)}. \end{cases} \tag{A.26}$$

Eqs. (A.25)–(A.26) give the (implicit) first-harmonic velocity response function. For a given Ω, the implicit equation for $\hat{V}$ can be solved through a bisection method, making using of intervals to confine the search for the roots of Eq. (A.25). The details of the numerical solution method are omitted here.

Data availability

Data will be made available on request.

References

[1] M. Murakawa, M. Jin, The utility of radially and ultrasonically vibrated dies in the wire drawing process, J. Mater. Process. Technol. 113 (1–3) (2001) 81–86.

[2] G. Eggers, J. Klein, J. Blank, S. Hassfeld, Piezosurgery: An ultrasound device for cutting bone and its use and limitations in maxillofacial surgery, Br. J. Oral Maxillofac. Surg. 42 (5) (2004) 451–453.

[3] Y. Ashida, H. Aoyama, Press forming using ultrasonic vibration, J. Mater. Process. Technol. 187 (2007) 118–122.

[4] A. Cabboi, M. Segeren, H. Hendrikse, A. Metrikine, Vibration-assisted installation and decommissioning of a slip-joint, Eng. Struct. 209 (2020) 109949.

[5] A. Cabboi, T. Kamphuis, E. van Veldhuizen, M. Segeren, H. Hendrikse, Vibration-assisted installation and decommissioning of a slip-joint: Application to an offshore wind turbine, Eng. Struct. 76 (2021).

[6] A. Tsetas, A. Tsouvalas, S.S. Gómez, F. Pisanò, E. Kementzetzidis, T. Molenkamp, A.S.K. Elkadi, A.V. Metrikine, Gentle driving of piles (GDP) at a sandy site combining axial and torsional vibrations: Part I - installation tests, Ocean Eng. 270 (113453) (2023).

[7] J. Monnoyer, E. Diaz, C. Bourdin, M. Wiertlewski, Optimal skin impedance promotes perception of ultrasonic switches, in: 2017 IEEE World Haptics Conference, WHC, IEEE, Munich, Germany, 2017, pp. 130–135.

[8] S. Matunaga, J. Onoda, New gravity compensation method by dither for low-g simulation, J. Spacecr. Rockets 32 (1995) 364–369.

[9] H. Storck, W. Littmann, J. Wallaschek, M. Mracek, The effect of friction reduction in presence of ultrasonic vibrations and its relevance to travelling wave ultrasonic motors, Ultrasonics 40 (1) (2002) 379–383.

[10] V. Kumar, I. Hutchings, Reduction of the sliding friction of metals by the application of longitudinal or transverse ultrasonic vibration, Tribol. Int. 37 (10) (2004) 833–840.

[11] J.J. Thomsen, Using fast vibrations to quench friction-induced oscillations, J. Sound Vib. 228 (5) (1999) 1079–1102.

[12] M.A. Michaux, A.A. Ferri, K. Cunefare, Effect of waveform on the effectiveness of tangential dither forces to cancel friction-induced oscillations, J. Sound Vib. 311 (3) (2008) 802–823.

[13] M. Leus, P. Gutowski, Analysis of longitudinal tangential contact vibration effect on friction force using Coulomb and dahl models, J. Theoret. Appl. Mech. 46 (1) (2008) 171–184.

[14] P. Gutowski, M. Leus, The effect of longitudinal tangential vibrations on friction and driving forces in sliding motion, Tribol. Int. 55 (2012) 108–118.

[15] P. Gutowski, M. Leus, Computational model for friction force estimation in sliding motion at transverse tangential vibrations of elastic contact support, Tribol. Int. 90 (2015) 455–462.

[16] P. Gutowski, M. Leus, Computational model of friction force reduction at arbitrary direction of tangential vibrations and its experimental verification, Tribol. Int. 143 (2020) 106065.

[17] E. Sulollari, K.N. van Dalen, A. Cabboi, Vibration-induced friction modulation for a general frequency of excitation, J. Sound Vib. 573 (2024).

[18] G. Amontons, De la resistance cause'e dans les machines (about resistance and force in machines), Mem L'Acedemie R A (1699) 257–282.

[19] C.A. Coulomb, Theorie Des Machines Simple (Theory of Simple Machines), Bachelier, Paris, 1821.

[20] A. Cabboi, J. Woodhouse, Validation of a constitutive law for friction-induced vibration under different wear conditions, Wear 396–397 (2018) 107–125.

[21] A. Cabboi, J. Woodhouse, Identifying short-term variation of dynamic friction by means of its frequency response function, J. Sound Vib. 472 (115212) (2020).

[22] J. Thomsen, Vibrations and Stability: Advanced Theory, Analysis, and Tools, Springer Verlag, Germany, 2003.

[23] F. Clementi, S. Lenci, G. Rega, 1:1 internal resonance in a two d.o.f. complete system: a comprehensive analysis and its possible exploitation for design, Meccanica 55 (6) (2020) 1309–1332.

[24] S. Kapelke, W. Seemann, On the effect of longitudinal vibrations on dry friction: Modelling aspects and experimental investigations, Tribol. Lett. 66 (3) (2018).

[25] M. Amabili, Nonlinear damping in nonlinear vibrations of rectangular plates: Derivation from viscoelasticity and experimental validation, J. Mech. Phys. Solids 118 (2018) 275–292.

[26] M. Amabili, Derivation of nonlinear damping from viscoelasticity in case of nonlinear vibrations, Nonlinear Dynam. 97 (2019) 1785–1797.

[27] M. Amabili, P. Balasubramanian, G. Ferrari, Nonlinear vibrations and damping of fractional viscoelastic rectangular plates, Nonlinear Dynam. 103 (2021) 3581–3609.